interaction of CD45 with its ligand may induce its dimerization and in turn regulate the activity of Lck. In the absence of ligand, both wild-type and mutant CD45 molecules are catalytically active monomers. In the presence of a CD45 ligand, both wild-type and mutant CD45 may dimerize, with different consequences for Lck activity. In cells expressing wild-type CD45, the catalytic site of each molecule would be blocked by the wedge containing glutamate 624 from the partner molecule, inhibiting CD45 phosphatase activity. Consequently, Lck would remain in the phosphorylated, inactive conformation, and TCR signals would be inhibited. In E624R-mutant CD45 molecules, the wedge is altered so that the catalytic sites are not occluded in the ligand-induced dimer. CD45 phosphatase activity would be retained and maintain Lck in its active conformation.

We chose to mutate glutamate 624 of CD45 because it is analogous to aspartate 228 within the putative inhibitory wedge of RPTPα (*8*). Aspartate 228 of one monomer contacts the mobile loop in the active site of the opposing monomer through a hydrogen bond between the side chain carboxyl moiety of aspartate 228 and a backbone amide of the loop. This interaction, along with other contacts, would preclude the necessary movement of the loop upon substrate binding, rendering the phosphatase inactive. Mutation of glutamate 624 of CD45 presumably disrupts the analogous interaction in CD45 dimers, thereby allowing the mobile loop to change conformation upon substrate binding, resulting in an active CD45 phosphatase.

Ligand-induced dimerization plays an essential role in the regulation of receptor tyrosine kinases, leading to autophosphorylation and activation of protein tyrosine kinase activity (*15*). Ligand-induced dimerization may also play an essential role in the regulation of RPTPs. However, instead of leading to activation, dimerization of RPTPs results in inhibition.

REFERENCES AND NOTES

1. R. J. Mourey and J. E. Dixon, *Curr. Opin. Genet. Dev.* **4**, 31 (1994); B. G. Neel and N. K. Tonks, *Curr. Opin. Cell Biol.* **9**, 193 (1997).
2. K. Kishihara *et al.*, *Cell* **74**, 143 (1993); K. F. Byth *et al.*, *J. Exp. Med.* **183**, 1707 (1996).
3. J. T. Pingel and M. L. Thomas, *Cell* **58**, 1055 (1989); I. S. Trowbridge and M. L. Thomas, *Annu. Rev. Immunol.* **12**, 85 (1994).
4. G. A. Koretzky, J. Picus, M. L. Thomas, A. Weiss, *Nature* **346**, 66 (1990).
5. A. C. Chan, D. M. Desai, A. Weiss, *Annu. Rev. Immunol.* **12**, 555 (1994).
6. H. L. Ostergaard *et al.*, *Proc. Natl. Acad. Sci. U.S.A.* **86**, 8959 (1989); E. D. McFarland *et al.*, *ibid.* **90**, 1402 (1993); M. Sieh, J. B. Bolen, A. Weiss, *EMBO J.* **12**, 315 (1993); T. R. Hurley, R. Hyman, B. M. Sefton, *Mol. Cell. Biol.* **13**, 1651 (1993).
7. D. M. Desai, J. Sap, J. Schlessinger, A. Weiss, *Cell* **73**, 541 (1993).
8. A. M. Bilwes, J. den Hertog, T. Hunter, J. P. Noel, *Nature* **382**, 555 (1996).
9. The EGFR-CD45 chimera (consisting of residues 1 through 646 of the human EGFR and residues 580 through 1281 of human CD45, numbered after the signal sequence from isoform ABC) has been described (*7*). The E624A and E624R mutations were introduced into the wild-type EGFR-CD45 chimera by oligonucleotide-based mutagenesis using the polymerase chain reaction and confirmed by nucleotide sequencing. H45.01 (*4*) cells (a CD45-deficient derivative of the HPB.ALL T cell line) were transfected with plasmids encoding the EGFR-CD45 mutant chimeric molecules. Subsequent limiting dilution and selection in geneticin-containing medium (2 mg/ml) yielded H45XLE624A.5 (expressing the EGFR-CD45/E624A mutant chimera) and H45XLE624R.3 (expressing the EGFR-CD45/E624R mutant chimera). H45XL2 (expressing the EGFR-CD45 wild-type chimera) was derived in a similar manner (*7*). Multiple clones expressing each of the chimeric molecules were isolated and analyzed.
10. R. Majeti and A. Weiss, data not shown.
11. D. M. Desai, J. Sap, O. Silvennoinen, J. Schlessinger, A. Weiss, *EMBO J.* **13**, 4002 (1994).
12. A. Weiss and D. R. Littman, *Cell* **76**, 263 (1994).
13. A. Takeda, J. J. Wu, A. L. Maizel, *J. Biol. Chem.* **267**, 16651 (1992).
14. J. A. Ledbetter, G. L. Schieven, F. M. Uckun, J. B. Imboden, *J. Immunol.* **146**, 1577 (1991); J. Marvel, G. Rimon, P. Tatham, S. Cockcroft, *Eur. J. Immunol.* **21**, 195 (1991); R. S. Mittler *et al.*, *J. Immunol.* **153**, 84 (1994).
15. J. Schlessinger and A. Ullrich, *Neuron* **9**, 383 (1992).
16. G. Grynkiewicz, M. Poenie, R. Y. Tsien, *J. Biol. Chem.* **260**, 3440 (1985).
17. D. Qian *et al.*, *J. Exp. Med.* **185**, 1253 (1997).
18. Cells were stained with a control monoclonal antibody (mAb) [goat antibody to mouse immunoglobulin G (Caltag Laboratories)]; with LA22 (antibody to EGFR; Upstate Biotechnology, Lake Placid, NY) for the EGFR-CD45 chimera; with Hle-1 (Becton-Dickinson) for CD45; and with Leu4 (antibody to CD3ε; Becton-Dickinson) for the TCR. Cells were stained at 4°C with saturating concentrations of fluorescein isothiocyanate (FITC)–conjugated primary antibody (control, Hle-1, and Leu4) or primary antibody (LA22) followed by FITC-conjugated goat antibody to mouse IgG. Cells were analyzed on a FACScan (Becton-Dickinson).
19. The intracellular free Ca^{2+} concentration was measured with the calcium-sensitive dye Indo-1 as described (*16*). Cells (5×10^6 per milliliter) were treated with antibody to CD3 (mAb 235 at a 1:3000 dilution of ascites) or EGF (100 ng/ml).
20. Cells were harvested, washed twice with phosphate-buffered saline (PBS), and resuspended at 2×10^8 per milliliter in PBS. Cells were incubated at 37°C for 15 min. For each sample, 2×10^7 cells were used, and an equal volume of stimulus in PBS warmed to 37°C was added for the indicated time so that final conditions were as follows: cells, 1×10^8 per milliliter; 235 ascites (mAb to CD3) at 1:500 dilution; and EGF, 100 ng/ml. Cells were sedimented in a microfuge and lysed in 200 μl of lysis buffer [1% Triton X-100, 150 mM NaCl, and 10 mM tris (pH 8.0), supplemented with protease and phosphatase inhibitors as described (*11*)]. Lysates were incubated at 4°C for 30 min, followed by centrifugation at 13,000*g* for 10 min. Ninety percent of the lysate was subjected to immunoprecipitation with polyclonal rabbit antibody to ZAP-70 [1598 (*17*)] and protein A–Sepharose beads for 2 hours at 4°C, after which immune complexes were washed. Immune complexes and 10% of the untreated lysate were resolved separately by SDS–polyacrylamide gel electrophoresis and transferred to polyvinylidene fluoride membranes (Millipore). Immunoblotting was done with mAb to phosphotyrosine (4G10; Upstate Biotechnology) or anti–phospho-MAPK (New England Biolabs), followed by visualization by enhanced chemiluminescence (Amersham). The blots were stripped and reprobed with antibody to ZAP-70 (1598) or antibody to MAPK (Santa Cruz Biotechnology), respectively.

21. We thank S. M. Fu for mAb 235, G. Servant for help with equilibrium binding studies, members of the Weiss lab for discussions and assistance, and A. DeFranco for his critical reading of this manuscript. Supported in part by a grant from NIH (to A.W.). R.M. is supported by the NIH Medical Scientist Training Program.

11 August 1997; accepted 6 November 1997

Dissociated Pattern of Activity in Visual Cortices and Their Projections During Human Rapid Eye Movement Sleep

Allen R. Braun,* Thomas J. Balkin, Nancy J. Wesensten, Fuad Gwadry, Richard E. Carson, Mary Varga, Paul Baldwin, Gregory Belenky, Peter Herscovitch

Positron emission tomography was used to measure cerebral activity and to evaluate regional interrelationships within visual cortices and their projections during rapid eye movement (REM) sleep in human subjects. REM sleep was associated with selective activation of extrastriate visual cortices, particularly within the ventral processing stream, and an unexpected attenuation of activity in the primary visual cortex; increases in regional cerebral blood flow in extrastriate areas were significantly correlated with decreases in the striate cortex. Extrastriate activity was also associated with concomitant activation of limbic and paralimbic regions, but with a marked reduction of activity in frontal association areas including lateral orbital and dorsolateral prefrontal cortices. This pattern suggests a model for brain mechanisms subserving REM sleep where visual association cortices and their paralimbic projections may operate as a closed system dissociated from the regions at either end of the visual hierarchy that mediate interactions with the external world.

Since its discovery in 1953 (*1*), the stage of sleep characterized by electroencephalographic desynchronization and rapid eye movements (REM sleep) has been the subject of unremitting scientific investigation. Exceptional interest in REM sleep

Table 1. Results of SPM contrasts and correlations between REMs and rCBF. Regions where rCBF values differ from baseline (REM-wake and REM-SWS) are tabulated with associated *Z*-scores and magnitude (Mag.) of rCBF differences (milliliters per 100 g per minute normalized to a mean of 50). Regions in which rCBF rates are correlated with REMs (REM Corrs) are tabulated with associated correlation coefficients. In each case Talaraich coordinates indicate local maxima or minima.

Regions	Brodman no.	REM-wake					REM-SWS					REM Corrs			
		X	*Y*	*Z*	Mag.	*Z*-score	*X*	*Y*	*Z*	Mag.	*Z*-score	*X*	*Y*	*Z*	*r*
Extrastriate cortex															
Fusiform, lingular gyrus	19, 37	24	−60	−8	4.22	3.10	−30	−54	−8	3.29	3.22*	−26	−60	−4	0.91†
Ventral lateral occipital–Inferotemporal cortex	19, 37	28	−66	4	2.62	3.30	−38	−58	−12	2.11	3.17	54	−50	0	0.95†
Lateral occipital–middle temporal cortex	18	32	−72	8	3.37	3.14						32	−82	8	0.83‡
Dorsal lateral occipital cortex	18, 19	34	−82	12	3.64	3.10						34	−72	12	0.71
Striate cortex															
Calcarine cortex	17						*10*	*−88*	*0*	*−9.30*	*−3.11*	*8*	*−82*	*0*	*−0.66*
Paralimbic cortex															
Parahippocampal gyrus–hippocampus	37	24	−20	−16	2.50	3.81	−24	−34	−4	4.33	3.12	32	−46	−8	0.83‡
Prefrontal cortex															
Lateral orbital cortex	10, 11, 47	*38*	*38*	*−12*	*−5.10*	*−3.63*	*−46*	*26*	*−4*	*−4.06*	*−4.07*	*−46*	*40*	*−4*	*−0.67*
Dorsolateral prefrontal cortex	9, 10, 46	*32*	*44*	*20*	*−2.78*	*−7.98*	*−44*	*8*	*24*	*−2.41*	*−3.10*	*−24*	*40*	*24*	*−0.73‡*

*Left hemisphere only. †$P < 0.001$. ‡$P < 0.01$ (otherwise $P < 0.05$).

has been sustained in part because it is the stage during which intense visual imagery-laden dream activity is most prevalent (*2*). However, the neural mechanisms that underlie generation of these images remain uncharacterized.

Although visual imagery (formation of an internally generated percept) and visual perception (representation of an externally generated stimulus) are behaviorally distinct, the extent to which this distinction is predicated on activation of different portions of the visual system is unclear.

It is not known, for example, whether images can be evoked at higher levels of the visual hierarchy—extrastriate cortices including V4, V5, inferotemporal and occipitoparietal processing pathways, and their anterior projections—or whether this process requires the contribution of early visual areas—V1 and V2 regions of the striate cortex—that are normally involved in primary visual perception.

Previous functional imaging studies, perhaps because they utilized different visual imagery–eliciting tasks during wakefulness, have produced contradictory results (*3*, *4*). Functional imaging during REM sleep affords a singular opportunity for study, because it is characterized by naturally occurring visual imagery–laden mentation and is defined by well-established, measurable criteria. Moreover, the functional anatomy of the visual system during REM sleep is of significant interest and may provide clues about the nature of this enigmatic "third state" of consciousness (*5*).

We used positron emission tomography (PET) and $H_2{}^{15}O$ to measure regional cerebral blood flow (rCBF) within visual cortices and their projections during REM sleep, compared with both wakefulness and stage 3–4 sleep [slow wave sleep (SWS)], and evaluated the regional cerebral correlates of the REMs that characterize this sleep stage.

Ten healthy male volunteers (*6*) underwent sleep deprivation and restriction pro-

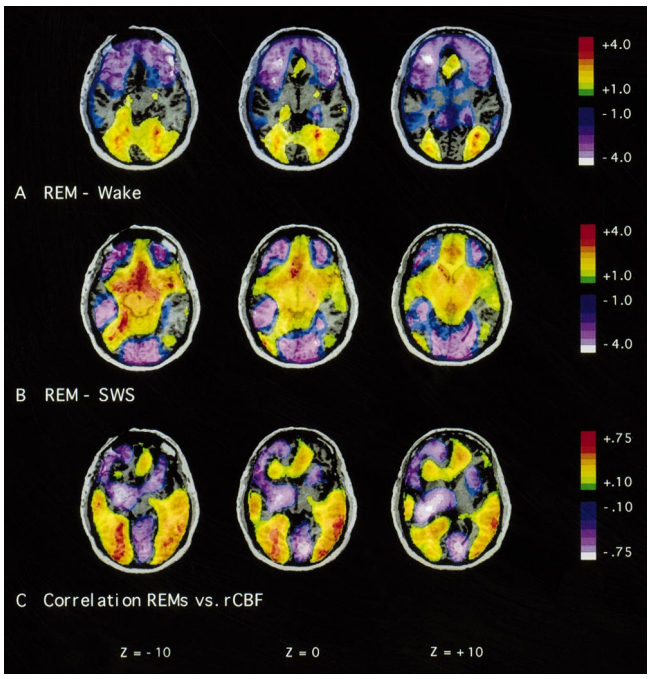

Fig. 1. Brain maps depicting changes in rCBF during REM sleep. Increases and decreases in rCBF during REM sleep compared with postsleep wakefulness (**A**) and SWS (**B**) are illustrated as well as positive and negative correlations between rCBF values and REM density (**C**). In (A) and (B) stage-specific changes in rCBF were evaluated for ANCOVA corrected data sets [see (*20*)]; the resulting SPM (*Z*) maps are displayed on a standardized magnetic resonance imaging (MRI) scan, which was transformed linearly into the same stereotaxic (Talairach) space as the SPM (*Z*) data. Planes of section are located at −10 mm (left), 0 mm (middle), and +10 mm (right) relative to the anterior commissural–posterior commissural line. Values are *Z*-scores representing the significance level of changes in normalized rCBF in each voxel; the range of scores is coded in the accompanying color table, with blue-white designating *Z*-scores of −4.0 and below and with dark red designating *Z*-scores of +4.0 and above. In (C) rapid conjugate eye movements recorded during the 180 s after the start of the scan were summed and correlated with normalized rCBF images on a pixel-by-pixel basis. The map illustrates these correlation coefficients displayed on the standardized MRI scan at the same planes of section. The range of coefficients is coded in the accompanying color table, with blue-white designating coefficients of −0.75 and below and with dark red designating coefficients of +0.75 and above. Location of local minima and maxima for *Z*-scores and correlation coefficients are summarized in Table 1.

A. R. Braun, F. Gwadry, M. Varga, Language Section, Voice Speech and Language Branch, National Institute on Deafness and Other Communication Disorders, National Institutes of Health, Bethesda, MD, USA.
T. J. Balkin, N. J. Wesensten, G. Belenky, Department of Neurobiology and Behavior, Division of Neuropsychiatry, Walter Reed Army Institute of Research, Washington, DC, USA.
R. E. Carson, P. Baldwin, P. Herscovitch, PET Imaging Section, Clinical Center, Building 10, Room 1C401, National Institutes of Health, Bethesda, MD 20892, USA.
*To whom correspondence should be addressed. E-mail: abraun@pop.nidcd.nih.gov

cedures (*7*) before the scanning session (*8*). Scans were performed during polysomnographically defined uninterrupted sleep stages 3–4 and during REM sleep (*9*). A waking study was performed at the end of the sleep period, after at least 15 min of continuous wakefulness.

Within-subject between-stage contrasts (REM-wake; REM-SWS) were analyzed by statistical parametric mapping (SPM) (*10*), and correlations between the frequency of REMs (REM density) and rCBF during REM sleep were examined (*11*). In addition, regional data were extracted from the PET images and analyzed by covariance techniques (principal component analyses and regional intercorrelations) to assess functional connections between regions of the brain (*12*).

Comparison of REM sleep and waking scans (Fig. 1A and Table 1) revealed focal activations of the extrastriate (fusiform, inferotemporal, and lateral occipital) cortices during REM sleep, manifest in clusters of significant spatial extent in both hemispheres (*13*). These clusters did not encompass the striate cortices (calcarine cortex and contiguous portions of the cuneus, as delimited in the Talairach atlas) where rCBF was unchanged compared with wakefulness. No hemispheral differences in the magnitude of rCBF activations were detected.

Because the use of resting scans as baseline may introduce a possible confound (*14*)—failure to detect differences in the primary visual cortex could be due to spontaneous production of visual imagery during waking scans acquired at rest—we contrasted REM sleep with SWS, a state in which spontaneous visual imagery is unlikely to have occurred (*15*).

This analysis not only confirmed the dissociation of activity in striate and extrastriate cortices but also showed that the striate cortex was deactivated during REM sleep compared with SWS (Fig. 1B and Table 1). Focal deactivation of the primary visual cortex was delimited in a single cluster of significant spatial extent (*16*). Furthermore, rCBF in the striate cortex was lower during REM sleep than during SWS even when absolute values corrected for partial pressure of CO_2 (PCO_2) were evaluated (although differences did not reach statistical significance) (*17*).

In contrast, rCBF in extrastriate cortices of the ventral processing stream—fusiform, inferotemporal, and ventral lateral occipital cortices—was significantly higher during REM sleep than during SWS [Fig. 1B and Table 1 (*Z*-scores exceeded threshold in the left hemisphere only)]; these regions were included in a larger cluster of significant activation (*18*). rCBF in regions of the dorsal processing stream was unchanged.

Contrasts of REM sleep with either wakefulness or SWS (Fig. 1, A and B and Table 1) also revealed significant changes in regions that represent principal targets of extrastriate projections, beyond the boundaries of the visual system (*19*). During REM sleep, activity in the parahippocampal gyri and the contiguous portions of the hippocampus increased in parallel with the extrastriate cortices, and rCBF in the ventrolateral (orbital) and dorsolateral prefrontal cortices was significantly decreased. There were no hemispheral differences in the magnitude of these changes (*20*).

The sleep-stage contrast results were closely paralleled by the spatial distribution of correlations between REM density and rCBF (Fig. 1C and Table 1); REM density was positively correlated with rCBF in extrastriate cortices in both hemispheres, particularly within ventral regions. In contrast, REM density was negatively correlated with rCBF in the striate cortices. In addition, REM density was positively correlated with rCBF in hippocampus and in parahippocampal gyri but was negatively correlated with rCBF in lateral orbital and dorsolateral prefrontal cortices.

Results of the principal component analysis are illustrated in Fig. 2. Striate and extrastriate regions loaded on the same component in both instances but with opposite signs—that is, across individuals increases in rCBF in extrastriate regions during REM sleep (compared with either wakefulness or SWS) were associated with concomitant decreases in the primary visual cortex. Permutation tests indicated that these components were significant in each instance ($P < 0.05$, exact), and the inverse relationship between striate and extrastriate loadings was stronger for ventral extrastriate regions (*21*). Inverse relationships between rCBF responses in selected regions of the extrastriate and striate cortices are illustrated in Fig. 3.

These results suggest that a functional dissociation between activity in the striate and extrastriate visual cortices characterizes, and may constitute a defining feature of, REM sleep. REM sleep was associated with selective activation of regions that are located in higher or "downstream" portions of the visual hierarchy. These include regions that may constitute human analogues of V4 and V5 as well as more anterior projections of ventral object-processing and dorsal spatial-processing pathways (*22*). REM-associated activation in most instances was more robust in extrastriate areas of the ventral stream. In contrast, the striate cortices were not activated, and most analyses suggested that rCBF in the primary visual cortex may be significantly attenuated during REM sleep.

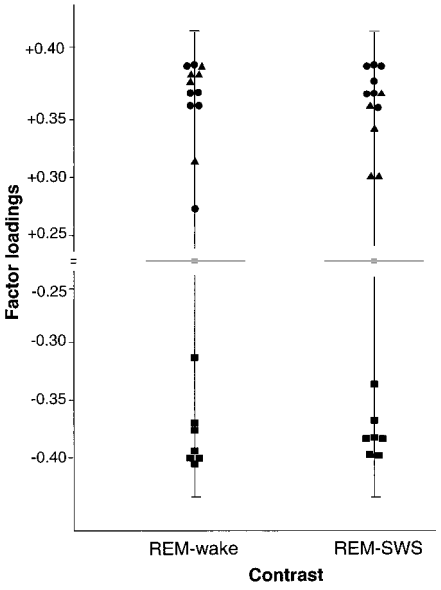

Fig. 2. Results of principal component analyses depicting the first unrotated component for REM-wake and REM-SWS. Principal component analysis was carried out on a difference matrix generated for each contrast. Values represent loadings for each of the 20 regions in which weights exceeded 0.25 in absolute value. Extrastriate areas: circles, fusiform-inferotemporal; triangles, lateral occipital. Striate areas: squares. The first component for REM-wake and REM-SWS contrasts accounted for 80.8% and 78.2% of the total variance, respectively.

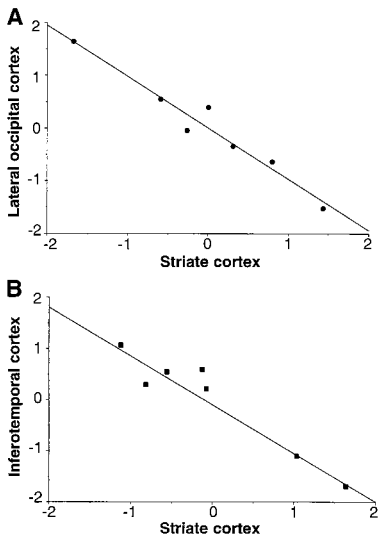

Fig. 3. Correlations between rCBF rates in striate and extrastriate cortices. Values represent standardized difference scores—that is, increases or decreases in rCBF during REM sleep compared with wake (**A**) and SWS (**B**), *Z*-transformed in each instance. rCBF responses in extrastriate (Talairach $x = -30$, $y = -88$, $z = -4$ in A; $x = -34$, $y = -58$, $z = -8$ in B) and striate ($x = -4$, $y = -80$, $z = -12$, both A and B) cortices were negatively correlated in both instances: $r^2 = 0.952$, REM-wake, $P < 0.001$; $r^2 = 0.914$, REM-SWS, $P < 0.001$.

These results were paralleled in the analysis of correlations between rCBF and REM density (*23*), suggesting a physiological mechanism that may mediate the effects of REM sleep on the visual cortex. In humans, REMs are associated with cerebral potentials that bear strong similarities to Pontogeniculooccipital (PGO) waves, which mediate the spontaneous central excitation of the visual cortices during REM sleep in animals (*24*). PGO waves may have a disproportionate effect on the excitability of extrastriate cortices, thus accounting for the relatively selective activation of these regions that was observed in this study (*25*).

REMs also serve as indices of dreaming: Although subjects were not awakened and debriefed in this study, REM density has been shown to correlate positively with the likelihood of dreaming, with the intensity and bizarreness of dream imagery, and with the presence of more vivid and visually active dreams (*26*). Our results thus suggest that the spontaneous generation of visual images that occurs during REM sleep may be associated with isolated activation of the extrastriate cortices (*27*).

Moreover, both principal component and correlation analyses, which may serve as a means of describing functional connections between brain regions, demonstrate a reciprocal relationship between activity in extrastriate and striate cortices during REM sleep, an observation that has not previously been described in PET studies of visual function during either waking or sleep (*28*–*30*).

What mechanism might account for this? It has been hypothesized that, because dreams typically consist of integrated and coherent visual images, there should be reentrant activation of the striate cortex by extrastriate back-projections during REM sleep, as has been suggested to occur during waking imagery tasks (*31*). Our results support an alternative hypothesis. Because increased synaptic activity in extrastriate areas is coupled to decreased activity in the primary visual cortex, firing of the extrastriate back-projections may in fact be attenuated—or actively inhibited—during REM sleep. Rather than leading to reentrant activation of V1 and V2, extrastriate activation during REM sleep may be linked to suppression of activity in primary regions connected to the external environment (*32*).

Indeed, REM sleep appears to be characterized by a double dissociation. Activity in extrastriate regions appears to be reciprocally related not only with activity in V1 and V2 but also with that in higher order frontal association areas to which extrastriate cortices project—dorsolateral prefrontal and lateral orbital cortices—heteromodal regions in which visual information is bound with that processed in other areas of the brain (*33*). At the same time, however, we observed concurrent activation of extrastriate regions and limbic-related projection areas—parahippocampal cortices and contiguous portions of the hippocampus—and activity in these mesial temporal regions was positively correlated with REM density. Of note, similar results were observed in the anterior cingulate cortex (Fig. 1), to which the parahippocampal cortices project.

This pattern suggests that pathways that mediate the transfer of information between visual cortices and the limbic system may be active during REM sleep, but pathways that mediate transfer of visual information to prefrontal association cortices are not.

Thus, during REM sleep, the extrastriate cortices and paralimbic areas to which they project may be operating as a closed system, functionally disconnected from frontal regions in which the highest order integration of visual information takes place. Such a dissociation could explain many of the experiential features of dreams, including heightened emotionality, uncritical acceptance of bizarre dream content, a dearth of parallel thoughts or images, temporal disorientation, and the absence of reflective awareness (*34*).

REM sleep may represent a state in which the brain engineers selective activation of an interoceptive network, which is dissociated from primary sensory and heteromodal association areas at either end of the visual hierarchy that mediate interactions with the external world.

REFERENCES AND NOTES

1. E. Aserinsky and N. Kleitman, *Science* **118**, 273 (1953).
2. W. Dement and N. Kleitman, *J. Exp. Psychol.* **53**, 339 (1957).
3. Some studies suggest that activation of only the higher levels of the visual processing hierarchy is sufficient to evoke and sustain visual imagery [P. E. Roland and B. Gulyas, *Cereb. Cortex* **5**, 79 (1995)].
4. Others [S. M. Kosslyn, W. L. Thompson, I. J. Kim, N. M. Alpert, *Nature* **378**, 496 (1995)] indicate that contribution of the primary visual processing areas—possibly activated through reentrant pathways [D. J. Felleman and D. C. Van Essen, *Cereb. Cortex* **1**, 1 (1991)]—is also required.
5. J. A. Hobson, *The Dreaming Brain* (Basic Books, New York, 1988).
6. Informed consent was obtained from 10 healthy male volunteers (23.6 ± 1.7 years of age, mean ± SD; range, 22 to 27 years). Eight subjects were right-handed, and two were left-handed.
7. There were 8 hours of sleep with selective REM deprivation on day 1; 2 hours of sleep with REM deprivation on day 2; and 15.5 to 23.5 hours of continuous wakefulness (22.2 ± 2.4 hours, mean ± SD) on day 3. Subjects were monitored polysomnographically throughout this period to verify the absence of sleep and facilitate selective REM deprivation.
8. PET scans were performed on a Scanditronix PC2048-15B tomograph (Uppsala, Sweden), which acquires 15 contiguous planes. A transmission scan was performed for attenuation correction.
9. A. Rechtschaffen and A. E Kales, *A Manual of Standardized Terminology, Techniques and Scoring System for Sleep Stages of Human Subjects* (Government Printing Office, Washington, DC, 1968). During all scans, subjects' eyes were closed and occluded by eye patches, and ambient noise was kept to an absolute minimum. When a target stage was identified, 30 mCi of $H_2{}^{15}O$ were injected and scans were initiated automatically. For inclusion in these analyses, a sleep stage had to be uniformly maintained (free of arousals and stage shifts) from 40 s before to 40 s after scan initiation. It was necessary to use partial sleep-deprivation methods to help ensure that subjects would sleep in the scanner. Such procedures, however, may affect sleep architecture (that is, the relative amounts and timing of the various stages within the sleep period). To evaluate these potential effects, we compared our subjects' sleep architecture with published normative data [R. L. Williams, I. Karacan, C. J. Hursch, *Electroencephalography (EEG) of Human Sleep: Clinical Applications* (Wiley, New York, 1974)]. Except for increased SWS time during the first third of the sleep period (an expected consequence of the deprivation procedure), we found no qualitative or quantitative abnormalities in the sleep architecture of our subjects. Furthermore, the scans selected for analysis were, in each instance, associated with sleep samples that conformed explicitly and unambiguously to the standard scoring criteria of Rechtschaffen and Kales throughout the period of data acquisition. Therefore, although sleep deprivation may have affected duration and timing of sleep stages, the procedure produced no observable effects on the physiological characteristics of the sleep stages themselves (that is, at the level of analysis most critical to this study).
10. PET scans were registered and normalized to a common stereotaxic space [J. Talairach and P. Tournoux, *Co-planar Stereotactic Atlas of the Human Brain* (Thieme, New York, 1988)], and stage-dependent differences in normalized rCBF were analyzed with SPM software [K. J. Friston, C. D. Frith, P. F. Liddle, R. S. J. Frackowiak, *J. Cereb. Blood Flow Metab.* **11**, 690 (1991)] with analysis of covariance (ANCOVA) correction for global blood flow. In addition, tests of significance based on the size of the activated region [K. J. Friston, K. J. Worsley, R. S. J. Frackowiak, J. C. Mazziotta, A. C. Evans, *Hum. Brain Mapp.* **1**, 210 (1994)] were performed; a Z-threshold of 2.33 and a value of $W = 2.73$ derived from a null contrast carried out in the same set of individuals were used. Absolute rCBF rates were also calculated by using a measured arterial input function and PCO_2 values. Of the 10 subjects in whom REM sleep scans were acquired, 7 had SWS scans, and 7 had waking postsleep studies. Stage contrasts were performed in a repeated measures design; thus, $N = 7$ for both REM-waking and REM-SWS contrasts. To evaluate hemispheral effects, differences in normalized rCBF for each contrast were compared between homologous pixels in right and left hemispheres by using a voxel-wise error variance; differences exceeding a Z-threshold of 3.09 were considered significant.
11. The frequency of rapid conjugate eye movements, identified as positive or negative deflections on the electrooculogram (EOG) during the 180 s after the start of the scan, were computed. Normalized rCBF images were correlated with each subject's REM counts on a pixel-by-pixel basis ($N = 10$ for these analyses) (Fig. 1C). Correlation coefficients were thresholded at a level of 0.6 ($P < 0.05$, $n = 10$) for tabulation (Table 1).
12. Coordinates for 20 visual cortical areas in each hemisphere (7 striate, 6 lateral occipital, 7 fusiform/inferotemporal) were selected by using the Talairach atlas, adjusted with the SPM PET template, and used to extract rCBF values from the stereotaxically normalized PET images. These values were normalized by using mean CBF rates for the visual cortex as a whole; rCBF values in homologous regions of right and left hemispheres were averaged and used to generate difference matrices (REM-SWS and REM-

wake; $N = 7$); a principal component analysis was then applied. Significance of the extracted component vector was assessed by using permutation tests [B. F. J. Manly, *Randomization and Monte Carlo Methods in Biology* (Chapman & Hall, New York, 1990)] by randomly permuting the sign of data entries 19 times; *P* values were derived by determining the proportion of permuted trials with higher first eigenvalues than the original data. Stability of regional loadings was assessed by the bootstrap procedure [B. Efron, *SIAM Monogr.* **38-I** (1982)]. Fit values of the original loadings across 10,000 bootstrap samples, expressed as *Z*-scores, were calculated; absolute values > 2.4 were considered stable.

13. Cluster 1, left hemisphere: 8688 mm^3; P' ($n_{max} > k$), corrected = 7.90×10^{-4}; centered $x = -4.9$, $y = -67.9$, $z = -5.3$; cluster 2, right hemisphere: 21056 mm^3; P' ($n_{max} > k$), corrected = 2.14×10^{-7}; centered $x = 21.9$, $y = -51.8$, $z = -6.8$.
14. S. M. Kosslyn and K. N. Ochsner, *Trends Neurosci.* **17**, 290 (1994).
15. A. Rechtschaffen, P. Verdone, J. Wheaton, *Can. Psychiatr. Assoc. J.* **8**, 409 (1963).
16. 17427 mm^3; P' ($n_{max} > k$), corrected = 1.90×10^{-6}; centered $x = 2.8$, $y = -83.0$, $z = 0.4$.
17. Absolute PCO_2 corrected flow rates were consistently lower during REM sleep than during SWS throughout the striate cortex [ΔrCBF = -6.40 ± 5.9 ml/100 g/min (mean ± SD), $x = 4$, $y = -82$, $z = 0$], and absolute rCBF rates were consistently elevated in extrastriate regions (in the fusiform cortex, ΔrCBF = $+8.85 \pm 2.79$ ml/100 g/min, $x = -34$, $y = -56$, $z = -8$), although variances in absolute values were large.
18. 58320 mm^3; P' ($n_{max} > k$), corrected = 3.55E −15; centered $x = -3.9$, $y = 0.3$, $z = 1.2$.
19. D. A. Chavis and D. N. Pandya, *Trans. Am. Neurol. Assoc.* **99**, 192 (1974); W. A. Suzuki and D. G. Amaral, *J. Comp. Neurol.* **350**, 497 (1994).
20. The frontal eye fields (superior dorsolateral prefrontal and premotor cortices) were incompletely sampled in many subjects and are not included in this analysis.
21. The bootstrapping procedures indicated that most regional loadings were stable. In the REM-SWS contrast, all the fusiform-inferotemporal regions—but none of the lateral occipital regions—were associated with *Z*-scores exceeding threshold (local maximum = 5.44, $x = \pm 48$, $y = -62$, $z = 0$). In the REM-wake contrast, six of the seven fusiform-inferotemporal regions (maximum 4.18, $x = \pm 48$, $y = -62$, $z = 4$), and four of the six lateral occipital regions (maximum 3.58, $x = \pm 32$, $y = -86$, $z = 0$) were stable; in the latter case, all were located in ventral rather than dorsal portions of the lateral occipital cortex ($z \leq 8$ mm). In the REM-SWS contrast, five of the seven striate loadings were stable (local minimum = −3.79, $x = \pm 4$, $y = -82$, $z = 0$), and in the REM-wake contrast, six of seven loadings were stable (minimum = −9.89, $x = \pm 4$, $y = -82$, $z = 0$).
22. S. Zeki *et al.*, *J. Neurosci.* **11**, 641 (1991); D. Watson *et al.*, *Cereb. Cortex* **3**, 79 (1993); J. V. Haxby *et al.*, *J. Neurosci.* **14**, 6336 (1994); I. Sereno *et al.*, *Science* **268**, 889 (1995).
23. These results could reflect the central effects of saccadic eye movements per se. Voluntary saccades during wakefulness previously have been found to be associated with reductions in visual CBF [T. Paus, S. Marrett, K. J. Worsley, A. C. Evans, *J. Neurophysiol.* **74**, 2179 (1995)]. However, saccades in that study were continuous and rapid (40 to 140 in 60 s) but were intermittent and lower in frequency in our own study [0 to 11 in 60 s (5.5 ± 4.0, mean ± SD]. Furthermore, reductions in rCBF were more widely distributed throughout the visual cortex, and no positive correlations between extrastriate activity and saccadic eye movements were observed, which suggests that the striate-extrastriate dissociation evident in this study may be a unique characteristic of REM sleep.
24. R. W. McCarley, J. W. Winkelman, F. H. Duffy, *Brain Res.* **274**, 359 (1983); C. W. Callaway, R. Lydic, H. A. Baghdoyan, J. A. Hobson, *Cell Mol. Neurobiol.* **7**, 105 (1987).
25. The effects of the PGO wave generator on the occipital cortex do not appear to be mediated through the lateral geniculate nucleus [J. A. Hobson, J. Alexander, C. J. Frederickson, *Brain Res.* **14**, 607 (1969)] and therefore are not expected to be exclusively associated with striate projections. Early studies also demonstrated that PGO wave amplitudes in the lateral association areas of the cat visual cortex exceed those in primary visual cortices [D. C. Brooks, *Exp. Neurol.* **22**, 603 (1968)], and single unit studies have shown that the facilitatory effects of PGO waves on neuronal firing rates appear to be manifest in extrastriate but not in striate cortices [T. Kasamatsu and W. R. Adey, *Brain Res.* **55**, 323 (1973)].
26. D. R. Goodenough, H. B. Lewis, A. Shapiro, I. Sleser, *J. Nerv. Ment. Dis.* **140**, 365 (1965); P. Verdone, *Percept. Mot. Skills* **20**, 1253 (1965); T. Pivik and D. Foulkes, *Science* **153**, 1282 (1966); W. Dement and E. A. Wolpert, *J. Exp. Psychol.* **55**, 543 (1958). See also (*2, 14*).
27. This appears to be consistent with the finding of Roland and Gulyas (*3*). However, our results may not be directly comparable with studies of conscious visual imagery; task-elicited activation of the primary visual cortex seen by Kosslyn *et al.* (*4*) might be a special feature of conscious visual imagery or retrieval processes that occur during the waking state.
28. P. Maquet *et al.* [*Nature* **383**, 163 (1996)] did not list rCBF changes in visual cortices; however, they compared REM sleep with an amalgam of wake and non-REM stages, whereas our contrasts were stage specific (for example, REM-SWS) and may be more sensitive.
29. P. L. Madsen *et al.* [*J. Cereb. Blood Flow Metab.* **11**, 502 (1991)] reported REM-associated increases in rCBF in visual association cortices; functional relationships between activity in striate and extrastriate cortices were not evaluated.
30. C. C. Hong *et al.* [*Sleep* **18**, 570 (1995)] reported a positive correlation between REM density and glucose metabolic rates in lateral occipital cortex, but results for primary visual cortex were not reported.
31. S. Zeki, *A Vision of the Brain* (Blackwell, Oxford, 1993). See also (*3, 4*).
32. A pattern of extrastriate activity in the absence of striate function also characterizes clinical states associated with unusual and often bizarre perturbations of visual awareness, such as blindsight [L. Weiskrantz, J. L. Barbur, A. Sahraie, *Proc. Natl. Acad. Sci. U.S.A.* **92**, 6122 (1995)] and confabulatory denial of blindness [G. Goldenberg, W. Mullbacher, A. Nowak, *Neuropsychologia* **33**, 1373 (1995)]. The features of both syndromes suggest that synchronous activation of primary and extrastriate cortices may be essential for "normal" visual awareness. That such coherence appears to be breached during REM sleep is not inconsistent with the altered awareness that characterizes this sleep stage.
33. Decreases in activity in the prefrontal cortex during REM sleep have been noted previously by Madsen *et al.* (*29*) and by Maquet *et al.* (*28*). On the other hand, Hong *et al.* (*30*) reported positive correlations between REM density and absolute glucose metabolic rates in the (right) dorsolateral prefrontal cortex; however, this measure, which reflects physiological responses over a longer time period, may not be directly comparable with normalized rCBF values evaluated in this study.
34. A. Rechtschaffen, *Sleep* **1**, 97 (1978); J. A. Hobson, *Endeavour* **20**, 86 (1996).
35. The authors wish to thank Dr. Alex Martin for his expertise, insight, and critical suggestions, which were essential in the preparation of this manuscript, and Dr. Scott Selbie for his valuable help in preparing Fig. 1.

11 August 1997; accepted 18 November 1997

Discrete Start Sites for DNA Synthesis in the Yeast *ARS1* Origin

Anja-Katrin Bielinsky and Susan A. Gerbi*

Sites of DNA synthesis initiation have been detected at the nucleotide level in a yeast origin of bidirectional replication with the use of replication initiation point mapping. The *ARS1* origin of *Saccharomyces cerevisiae* showed a transition from discontinuous to continuous DNA synthesis in an 18–base pair region (nucleotides 828 to 845) from within element B1 toward B2, adjacent to the binding site for the origin recognition complex, the putative initiator protein.

An origin of bidirectional DNA replication is characterized by the transition between continuous DNA synthesis (proceeding in one direction) and discontinuous synthesis (proceeding in the opposite direction). We have developed replication initiation point (RIP) mapping to determine this transition in the autonomously replicating sequence (ARS) 1 of the yeast *Saccharomyces cerevisiae*.

ARS1 functions as an origin of DNA replication (ORI) both on a plasmid and in its normal context on chromosome IV (*1*). *ARS1*-containing plasmids respond normally to the cell cycle, duplicating once per cycle (*2*), and replication is initiated by the same cellular protein machinery acting on chromosomes.

ARS1 is composed of subdomains A, B1, B2, and B3 (*3*). Subdomains A and B1 are recognized by the origin recognition complex (ORC) (*4*), the putative initiator protein (*5*) indispensable for origin function (*6, 7*). Element B2 is easily unwound DNA (*8*) and element B3 is a binding site for the ARS binding factor I (ABFI) (*9*).

RIP mapping, described here, has sufficient sensitivity for study of eukaryotic origins, unlike an earlier method (*10*). It allows precise mapping of initiation sites for DNA synthesis and was applied to a

Department of Molecular Biology, Cell Biology and Biochemistry, Division of Biology and Medicine, Brown University, Providence, RI 02912, USA.

*To whom correspondence should be addressed. E-mail: susan_gerbi@brown.edu